



Short communication

High Li⁺ conduction in NASICON-type Li_{1+x}Y_xZr_{2-x}(PO₄)₃ at room temperatureYutao Li^a, Meijing Liu^{a,b}, Kai Liu^a, Chang-An Wang^{a,*}^aState Key Laboratory of New Ceramics and Fine Processing, School of Materials Science and Engineering, Tsinghua University, Beijing 100084, PR China^bSchool of Materials Science and Engineering, Jingdezhen Ceramic Institute, Jingdezhen, Jiangxi 333001, PR China

HIGHLIGHTS

- The rhombohedral NASICON Li_{1+x}Y_xZr_{2-x}(PO₄)₃ (0.1 ≤ x ≤ 0.2) was stabilized at 25 °C.
- The bulk conductivity of Li_{1.15}Y_{0.15}Zr_{1.85}(PO₄)₃ were 1.4 × 10⁻⁴ S cm⁻¹ at 25 °C.
- The activation energy was about 0.39 eV in the temperature range 300–473 K.
- The dopant Y³⁺ reduces the size of the interstitial space in the M1 cavity.
- The size change in M1 and M2' cavity facilitates the Li⁺ transport.

ARTICLE INFO

Article history:

Received 19 December 2012

Received in revised form

10 March 2013

Accepted 29 March 2013

Available online 8 April 2013

Keywords:

Li solid electrolyte

NASICON

Li-ion battery

Ionic conductivity

ABSTRACT

The NASICON oxides with general formula Li_{1+x}Y_xZr_{2-x}(PO₄)₃ (0.1 ≤ x ≤ 0.2) are prepared by conventional solid-state reaction. The samples are characterized by XRD, SEM, electrochemical impedance spectroscopy and ⁷Li MAS NMR measurements. The structures are refined by the Rietveld method from powder X-ray diffraction data. With the introduction of Y³⁺, the volume of the large M1 cavity is reduced and the rhombohedral NASICON phase is stabilized at room temperature. The bulk and total Li⁺ conductivities of Li_{1.15}Y_{0.15}Zr_{1.85}(PO₄)₃ sintered by SPS are 1.4 × 10⁻⁴ and 0.71 × 10⁻⁴ S cm⁻¹ at 25 °C, respectively; the activation energy is about 0.39 eV in the temperature range 300–473 K.

© 2013 Elsevier B.V. All rights reserved.

1. Introduction

Limitations of the flammable organic liquid-carbonate electrolytes of the Li-ion batteries and interest in Li-ion batteries using a solid separator of an organic-liquid electrolyte on the anode side and an aqueous or air cathode has stimulated the search for Li-ion solid electrolytes having a room-temperature Li⁺ conductivity $\sigma_{\text{Li}} > 10^{-4}$ S cm⁻¹ [1,2]. At present, slightly-modified Li_{1.3}Ti_{1.7}Al_{0.3}(PO₄)₃ with rhombohedral NASICON structure [3,4] is the best commercially available oxide Li-ion solid electrolyte. Solid alkali-ion conductors with NASICON structure have been thoroughly investigated from both the structural and electrical points of view [5–8].

The crystal structure of NASICON A_xB₂(PO₄)₃ is a framework built of corner-sharing PO₄ tetrahedra and BO₆ octahedra, providing a relatively open, three-dimensional network of sites and conduction pathways for various A cations. Two main types of cavities, denoted M1 and M2, are generally considered, the former is a six-coordinate site while the latter is an irregular eight-coordinate site. The most important system of the family is LiZr₂(PO₄)₃, which can be expected to be electrochemically stable on contact with lithium metal. The NASICON LiZr₂(PO₄)₃ compound prepared at 1473 K exhibits a first order transition from the triclinic C1> to the rhombohedral R3c form at about 310 K [9], and the rhombohedral phase R3c with high Li⁺ conductivity can be stable only above 50 °C. The Li⁺ conductivities of the triclinic and rhombohedral phases are $\sigma_{\text{Li}} = 5 \times 10^{-8}$ S cm⁻¹ at 25 °C and $\sigma_{\text{Li}} \approx 1 \times 10^{-5}$ S cm⁻¹ close to room temperature, respectively [10,11].

In our previous work we reported that the substitution of 5% of Ca²⁺ for Zr⁴⁺ in LiZr₂(PO₄)₃ can transform the structure to rhombohedral NASICON at room temperature and increase the ionic

* Corresponding author.

E-mail address: lytthu@gmail.com (C.-A. Wang).

conductivity significantly [12,13]. The Li^+ conductivity in NASICON $\text{LiZr}_2(\text{PO}_4)_3$ should be further improved through optimizing the doping element and content to increase the density of the bulk material and tune the size of the interstitial channel for Li^+ conduction. Here we find that with the introduction of Y^{3+} , the rhombohedral phase can be stabilized at room temperature; the bulk and total Li^+ conductivities of $\text{Li}_{1.15}\text{Y}_{0.15}\text{Zr}_{1.85}(\text{PO}_4)_3$ sintered by Spark Plasma Sintering (SPS) at 1200 °C were 1.4×10^{-4} and $0.71 \times 10^{-4} \text{ S cm}^{-1}$ at 25 °C, respectively.

2. Experimental

Compounds with the chemical formula $\text{Li}_{1+x}\text{Y}_x\text{Zr}_{2-x}(\text{PO}_4)_3$ ($0.1 \leq x \leq 0.2$) were prepared by solid-state reaction of stoichiometric amounts of Li_2CO_3 , Y_2O_3 , ZrO_2 and $(\text{NH}_4)_2\text{HPO}_4$. The powders were ball-milled with zirconia balls and heated to 900 °C to decompose the metal salts. The resultant product was ball-milled and sintered at 1200 °C for 20 h. Finally the powders were ball-milled again and pressed into a pellet under 40 MPa and then annealed at 1200 °C for 18 h in air; for $x = 0.2$, the samples were ball-milled again and fired at 1200 °C for 18 h to get the NASICON phase. The annealing was done in a platinum crucible. To increase the density of the samples, the powders after sintering at 1200 °C for 18 h were sintered by SPS at 1200 °C for 20 min under 40 MPa.

Powder X-ray diffraction (D8 advance A25, Cu $\text{K}\alpha$) was employed to monitor the phase formation in the 2θ range from 10° to 70° with a step size of 0.02°. Structural refinements of the resulting compounds were performed with Fullprof software. A field-emission scanning electron microscope (Quanta FEG650) was used to obtain the fracture surface microstructure of the pellet. The composition distribution of the elements was measured by inductively coupled plasma-optical emission spectroscopy (ICP-OES). A differential scanning calorimeter (DSC Q200) was used to analyze the phase transformation of $\text{Li}_{1+x}\text{Y}_x\text{Zr}_{2-x}(\text{PO}_4)_3$ ($0.1 \leq x \leq 0.2$). The experiment was carried out under a static air atmosphere between –90 and 200 °C with a heating rate of 2 °C min^{-1} .

${}^7\text{Li}$ NMR spectra recorded under MAS condition were obtained at room temperature using a B-VT 1000/SU07 unit adapted to advance III 400 Bruker spectrometer. The frequency used for ${}^7\text{Li}$ was 155.50 MHz. Spectra were taken after a $\pi/2$ pulse irradiation and the interval between successive scans chosen to avoid saturation effects (20–30 s), the spinning rate of samples was 12 kHz and the number of accumulations was 4. ${}^7\text{Li}$ chemical shift values were given relative to 1 M LiCl aqueous solutions.

Ionic conductivity was measured from 300 to 473 K with an Agilent 4294A Impedance Analyzer; the applied frequency range was from 110 MHz to 100 Hz with a 5 mV AC amplitude. Both parallel surfaces of the pellet were sputtered with Li-ion-blocking Au electrodes.

3. Results

Fig. 1 shows the powder XRD patterns after pressureless sintering and SPS. The diffraction peaks observed were assigned to a well-crystallized rhombohedral NASICON structure. Only a very small amount of YPO_4 exists in $\text{Li}_{1+x}\text{Y}_x\text{Zr}_{2-x}(\text{PO}_4)_3$ compound with $x = 0.15$ and 0.2. An amorphous secondary phase (e.g. P_2O_5 or Li_3PO_4) was easily formed during the synthesis of $\text{LiZr}_2(\text{PO}_4)_3$, which was confirmed by ${}^{31}\text{P}$ NMR experiments [9,14]. The lattice parameters, cell volume of $\text{Li}_{1+x}\text{Y}_x\text{Zr}_{2-x}(\text{PO}_4)_3$ obtained by Rietveld refinement and structural data of $\text{LiZr}_2(\text{PO}_4)_3$ extrapolated to room temperature from the thermal-expansion data [6] above 150 °C are listed in Table 1S. The substitution of Zr^{4+} by Y^{3+} in $\text{LiZr}_2(\text{PO}_4)_3$ causes an increase of the lattice parameters and cell volume of the

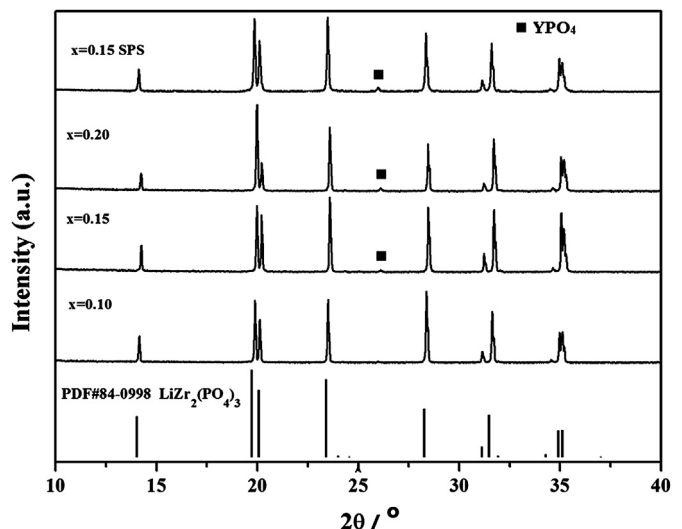


Fig. 1. XRD patterns of $\text{Li}_{1+x}\text{Y}_x\text{Zr}_{2-x}(\text{PO}_4)_3$ ($0.1 \leq x \leq 0.2$) after pressureless sintering and SPS.

$\text{Li}_{1+x}\text{Y}_x\text{Zr}_{2-x}(\text{PO}_4)_3$ compound. The variations can be caused by the different values of ionic radii of Zr^{4+} (0.72 Å) and Y^{3+} (0.88 Å) ions, and more Li^+ is needed to compensate for the charge balance after the substitution. The lattice parameter c in $\text{Li}_{1.2}\text{Y}_{0.15}\text{Zr}_{1.8}(\text{PO}_4)_3$ is a little smaller than that in $\text{Li}_{1.15}\text{Y}_{0.15}\text{Zr}_{1.85}(\text{PO}_4)_3$, which maybe caused by the different sintering process. Calorimetric curves obtained during the heating runs of $\text{Li}_{1+x}\text{Y}_x\text{Zr}_{2-x}(\text{PO}_4)_3$ with $x = 0.1$ and 0.15 are shown in Fig. 1S, no endothermic peak was detected, which indicate that there is no first order transition from the rhombohedral $R\bar{3}c$ to the triclinic $C\bar{T}$ phase. With the introduction of Y^{3+} , the rhombohedral NASICON phase can be stable even at –90 °C. The molar ratio of $\text{Li}^+:\text{Y}^{3+}:\text{Zr}^{4+}$ elements was 1.12:0.14:1.87 for $x = 0.15$, which is in good agreement with the general formula $\text{Li}_{1.15}\text{Y}_{0.15}\text{Zr}_{1.85}(\text{PO}_4)_3$.

Fig. 2S displays the fractural microstructure of the pellet after sintering. The particles are in good contact with each other, and a certain amount of pores in the boundary area after pressureless sintering can be observed. The $\text{Li}_{1+x}\text{Y}_x\text{Zr}_{2-x}(\text{PO}_4)_3$ samples sintered by SPS at 1200 °C for 20 min shows better connection and less amount of pores, which can reduce the grain-boundary resistance. The densities of ceramics with $x = 0.15$ sintered by pressureless sintering at 1200 °C for 18 h and SPS at 1200 °C for 20 min were about 85% and 90% of the theoretical densities, respectively.

An impedance spectrum of the prepared $\text{Li}_{1+x}\text{Y}_x\text{Zr}_{2-x}(\text{PO}_4)_3$ pellet for $x = 0.15$ measured at 25 °C is exhibited in Fig. 2(a). The appearance of a low-frequency tail in the case of ionically blocking electrodes is an indication that the conductivity of $\text{Li}_{1+x}\text{Y}_x\text{Zr}_{2-x}(\text{PO}_4)_3$ is ionic in nature. The bulk and grain-boundary resistance could be obtained by fitting the experimental data with the conventional equivalent circuit consisting of $(R_b\text{CPE1})(R_{gb}\text{CPE2})(\text{CPE3})$. The optimized bulk and total conductivities at 25 °C after pressureless sintering are 1.4×10^{-4} and $0.31 \times 10^{-4} \text{ S cm}^{-1}$ in $\text{Li}_{1+x}\text{Y}_x\text{Zr}_{2-x}(\text{PO}_4)_3$ with $x = 0.15$, and the total conductivity can be further improved to $0.71 \times 10^{-4} \text{ S cm}^{-1}$ for samples sintered by SPS at 1200 °C for 20 min for with $x = 0.15$, which is higher than that of our previous report on $\text{Li}_{1.2}\text{Ca}_{0.1}\text{Zr}_{1.9}(\text{PO}_4)_3$ [12,13] and is comparable to that of Al^{3+} -contaminated “ $\text{Li}_7\text{La}_3\text{Zr}_2\text{O}_{12}$ ” [15]. The grain-boundary contribution to the total resistance is appreciable and amounts to about 77% and 51% at 25 °C sintered by pressureless sintering and SPS, respectively. The bulk and total conductivities at 25 °C in $\text{Li}_{1+x}\text{Y}_x\text{Zr}_{2-x}(\text{PO}_4)_3$ with different x are shown in Table 2S,

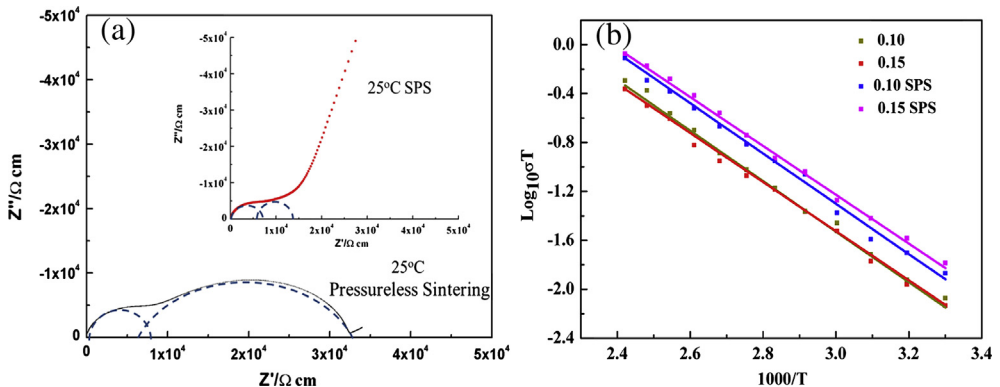


Fig. 2. (A) Impedance plot (100 Hz–110 MHz) of $\text{Li}_{1+x}\text{Y}_x\text{Zr}_{2-x}(\text{PO}_4)_3$ with $x = 0.15$ measured in air by pressureless sintering and SPS. (B) Temperature dependence of lithium conductivity of $\text{Li}_{1+x}\text{Y}_x\text{Zr}_{2-x}(\text{PO}_4)_3$ with $x = 0.1$ and 0.15.

the bulk conductivities in $\text{Li}_{1+x}\text{Y}_x\text{Zr}_{2-x}(\text{PO}_4)_3$ are much higher than that in $\text{LiZr}_2(\text{PO}_4)_3$ with NASICON structure near room temperature ($\sigma_{\text{Li}} \approx 1 \times 10^{-5} \text{ S cm}^{-1}$).

Fig. 2b shows the Li^+ conductivity as a function of 1000 T^{-1} for a sintered sample of $\text{Li}_{1+x}\text{Y}_x\text{Zr}_{2-x}(\text{PO}_4)_3$ ($x = 0.10$ and 0.15). The temperature dependence of the conductivity can be expressed by the Arrhenius equation.

$$\sigma T = A \exp(-E_a/kT)$$

The activation energy was estimated to be $E_a = 0.40$ and 0.39 eV sintered by pressureless sintering and SPS from the slope of the $\log \sigma T$ versus 1000 T^{-1} plot in the temperature range of 300–473 K with $x = 0.10$ and 0.15. The activation energy for the total lithium-ion conductivity is smaller than that in rhombohedral $\text{Li}_2\text{Zr}(\text{PO}_4)_3$ (0.43 eV) [9]. The activation energy for the total lithium-ion conductivity is comparable to Ca^{2+} -doping $\text{Li}_2\text{Zr}(\text{PO}_4)_3$ [11,12] and fast Li^+ garnet conductors such as $\text{Li}_6\text{BaLaTa}_2\text{O}_{12}$ [16] (0.40 eV), $\text{Li}_7\text{La}_3\text{Zr}_2\text{O}_{12}$ [17] (0.30 eV).

4. Discussion

To clarify the influence of the doping Y^{3+} on the NASICON structure and the Li^+ transport within the framework, the refinement of $\text{Li}_{1.15}\text{Y}_{0.15}\text{Zr}_{1.85}(\text{PO}_4)_3$ structure was done using the Rietveld

analysis of powder X-ray diffraction patterns. The localisation of Li atoms using the X-ray diffraction technique is not efficient due to their low X-ray scattering factor, therefore, only the atomic positions of Zr(Y), P and O atoms within the framework and their anisotropic atomic displacement factors were refined in the refinement. Linear interpolation between a set background points with refinable heights was used to model the intensity background, and the peak shape was represented by a convolution of a pseudo-Voigt function, and the occupancy of Zr atom was also refined.

The crystal structure of $\text{LiZr}_2(\text{PO}_4)_3$ at 873 K in which the lithium was disordered with occupancies of 7% tetrahedral sites (18e) and 13% tetrahedral sites (36f) was adopted as the initial structure model. This refinement led to a rather good agreement between the experimental and the calculated XRD patterns (Fig. 3) and to low reliability factors ($R_{\text{wp}} \sim 11.0\%$; $R_{\text{B}} \sim 2.3\%$). Our rhombohedral NASICON $\text{Li}_{1.15}\text{Y}_{0.15}\text{Zr}_{1.85}(\text{PO}_4)_3$ had space group $R\bar{3}c$ with lattice parameter $a = 8.8727$ and $c = 22.1578 \text{ \AA}$. In NASICON $\text{LiB}_2(\text{PO}_4)_3$, Li^+ moves in the $\text{B}_2(\text{PO}_4)_3$ framework, which contains an array of M1 interstitial sites separated by an array of M2 interstitial sites, and there are three times as many M2 as M1 sites. The Li^+ only occupies the M1 site in $\text{LiTi}_2(\text{PO}_4)_3$ [5] while in $\text{LiZr}_2(\text{PO}_4)_3$ about 90% Li^+ occupies the 6-fold disordered 36f tetrahedral site (displaced from M1 site) in M1 cavity and about 10% Li^+ occupies the 3-fold disordered 18e tetrahedral sites (displaced from M2 site) in M2' cavity (Fig. 4) at 423 K [6]. The tunnels in $\text{LiZr}_2(\text{PO}_4)_3$ are not suitable

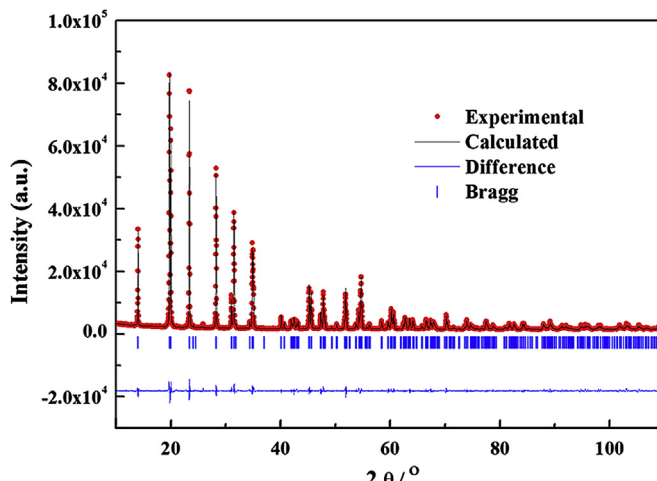


Fig. 3. Observed, calculated, and difference profiles of powder diffraction patterns of NASICON $\text{Li}_{1.15}\text{Y}_{0.15}\text{Zr}_{1.85}(\text{PO}_4)_3$.

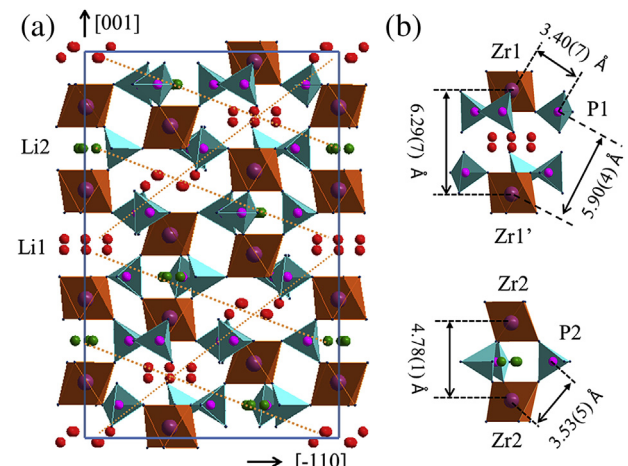


Fig. 4. (a) Unit-cell of $\text{Li}_{1.15}\text{Y}_{0.15}\text{Zr}_{1.85}(\text{PO}_4)_3$ projected onto the (110) plane. (b) The M1 and M2' cavity within $\text{Li}_{1.15}\text{Y}_{0.15}\text{Zr}_{1.85}(\text{PO}_4)_3$.

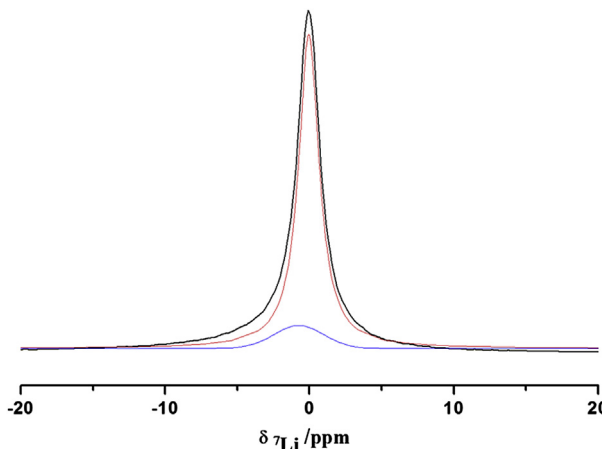


Fig. 5. ${}^7\text{Li}$ MAS NMR spectra of $\text{Li}_{1.15}\text{Y}_{0.15}\text{Zr}_{1.85}(\text{PO}_4)_3$ at room temperature, the line shape is fit as a sum of broad and narrow component associated with slow and fast lithium ion domains.

in size for small Li^+ ion migration, and the ionic conductivity of the system is greatly increased when Zr^{4+} in $\text{LiZr}_2(\text{PO}_4)_3$ is substituted by a smaller Ti^{4+} ion [18].

Close examination of the atomic positions and interatomic distances shows that the main difference between $\text{Li}_{1.15}\text{Y}_{0.15}\text{Zr}_{1.85}(\text{PO}_4)_3$ at 25 °C and $\text{LiZr}_2(\text{PO}_4)_3$ structures at different temperatures (150, 400 and 600 °C) is the size of M1 and M2' cavity. The $\text{Zr}(1)-\text{Zr}(1')$, $\text{Zr}(1)-\text{P}(1)$ and $\text{Zr}(1')-\text{P}(1)$ interatomic distances in $\text{Li}_{1.15}\text{Y}_{0.15}\text{Zr}_{1.85}(\text{PO}_4)_3$ (6.2972, 3.4076 and 5.9048 Å) in Fig. 4 are much shorter than the corresponding $\text{Zr}(1)-\text{Zr}(1')$, $\text{Zr}(1)-\text{P}(1)$ and $\text{Zr}(1')-\text{P}(1)$ distances in $\text{LiZr}_2(\text{PO}_4)_3$ [6] at different temperatures (e.g. 6.4115, 3.4374, and 5.9809 Å at 600 °C); moreover the P–O and Zr–O bond lengths also increase in $\text{Li}_{1.15}\text{Y}_{0.15}\text{Zr}_{1.85}(\text{PO}_4)_3$, so the volume of the six-coordinated M1 cavity decreases, and then less thermal energy is needed to push the mobile Li^+ into the center of the diffusion pathway. The Li ions which reside in the 6-fold disordered 36f tetrahedral sites in M1 cavity play a major role in the mobile process [6], so the reduced interstitial space will lead to more suitable tunnel for Li^+ transport. The $\text{Zr}(2)-\text{P}(2)$ interatomic distances (3.535 Å) are significantly longer than the corresponding $\text{Zr}(2)-\text{P}(2)$ distances (e.g. 3.4953 Å at 600 °C) in $\text{LiZr}_2(\text{PO}_4)_3$; a little increase in the $\text{Zr}(2)-\text{Zr}(2)$ distances (4.7817 Å) in parallel to c -axis is observed for $\text{Li}_{1.15}\text{Y}_{0.15}\text{Zr}_{1.85}(\text{PO}_4)_3$ at room temperature in comparison to what is observed for $\text{LiZr}_2(\text{PO}_4)_3$ at 150 °C (4.7698 Å) and 400 °C (4.7798 Å). The volume of M2' cavity increases, therefore, the Li–O distances increase. The Li ion in the 18e tetrahedral sites inside M2' cavity in $\text{LiZr}_2(\text{PO}_4)_3$ is bonded to oxygens strongly due to the short Li–O distances, and in $\text{Li}_{1.15}\text{Y}_{0.15}\text{Zr}_{1.85}(\text{PO}_4)_3$, the Li ions inside M2' cavity will be activated and contribute to Lithium transport within the framework, due to the bigger size of M2' cavity and longer Li–O distance. The size change in M1 and M2' cavity makes an indirect mechanism involving Li2 as intermediate site possible and even Li^+ redistribution in 18e and 36f tetrahedral sites. The ZrO_6 octahedra in $\text{Li}_{1.15}\text{Y}_{0.15}\text{Zr}_{1.85}(\text{PO}_4)_3$ exhibit six almost similar Zr–O distances (2.07(0), 2.07(9) Å), due to the size change in M1 and M2' cavity, and are less distorted than that in $\text{LiZr}_2(\text{PO}_4)_3$ at 150 °C, where $\text{Li}(2)$ gets closer to $\text{Zr}2$. The P–O distance in $\text{Li}_{1.15}\text{Y}_{0.15}\text{Zr}_{1.85}(\text{PO}_4)_3$ (1.52(8), 1.53(5) Å) are in good agreement with those typically observed in NASICON-type structure.

${}^7\text{Li}$ MAS NMR technique was used to probe Li dynamics in NASICON $\text{Li}_{1.15}\text{Y}_{0.15}\text{Zr}_{1.85}(\text{PO}_4)_3$. In Fig. 5, The ${}^7\text{Li}$ NMR spectrum displayed a central transition ($-1/2 \rightarrow 1/2$) resonance

at -0.02 ppm; the two-component NMR line was represented by a composite of a broad (Gaussian) and a narrow (Lorentzian) component, which can be assigned to ${}^7\text{Li}$ populations with higher and lower ion mobilities [19,20]. The area fraction (A_f) of the narrow contribution, representing fast Li ions in $\text{Li}_{1.15}\text{Y}_{0.15}\text{Zr}_{1.85}(\text{PO}_4)_3$, amounts to approximately 91%.

The size change in M1 and M2' cavity shortened the distance between the Li^+ ions inside M1 cavity (roughly 3.83(4) Å in $\text{Li}_{1.15}\text{Y}_{0.15}\text{Zr}_{1.85}(\text{PO}_4)_3$ compared to 4.29(1) Å in $\text{LiZr}_2(\text{PO}_4)_3$ at 150 °C) and facilitated the Li^+ transport in the mobile path along $\text{Li}1-\text{Li}1'-\text{Li}1' \dots$ network inside the NASICON structure. Doping with Y^{3+} also increases 15% Li^+ concentration in the interstitial space, which introduces Li^+ into interstitial $\text{Li}1$ and $\text{Li}2$ sites and lowers the motional enthalpy E_a by introducing Li^+-Li^+ coulombic interactions to displace the Li^+ ions from the interstitial $\text{Li}1$ sites.

5. Conclusions

The NASICON oxides with general formula $\text{Li}_{1+x}\text{Y}_x\text{Zr}_{2-x}(\text{PO}_4)_3$ ($0.1 \leq x \leq 0.2$) were prepared by conventional solid-state reaction. With the introduction of Y^{3+} , the rhombohedral NASICON phase was stabilized at room temperature. The bulk and total lithium ion conductivities of $\text{Li}_{1.15}\text{Y}_{0.15}\text{Zr}_{1.85}(\text{PO}_4)_3$ sintered by SPS at 25 °C were 1.4×10^{-4} S cm $^{-1}$ and 0.71×10^{-4} S cm $^{-1}$, respectively; the activation energy was about 0.39 eV in the temperature range 300–500 K. The dopant Y^{3+} reduces the size of the interstitial space in the M1 cavity, and the size change in M1 and M2' cavity facilitates the Li^+ transport within the NASICON framework.

Acknowledgement

This work was supported by the National Natural Science Foundation of China (Grant No: 50921061 and 51221291).

Supplementary data

Supplementary data related to this article can be found at <http://dx.doi.org/10.1016/j.jpowsour.2013.03.175>.

References

- [1] J.B. Goodenough, Y. Kim, Chemistry of Materials 22 (2010) 587–603.
- [2] Y. Lu, J.B. Goodenough, Y. Kim, Journal of the American Chemical Society 133 (2011) 5756–5759.
- [3] H. Aono, et al., Journal of the Electrochemical Society 137 (1990) 1023–1027.
- [4] H. Aono, et al., Chemistry Letters 10 (1990) 1825–1828.
- [5] A. Aatiq, et al., Journal of Materials Chemistry 12 (2002) 2971–2978.
- [6] M. Catti, A. Comotti, S. Di Blas, Chemistry of Materials 15 (2003) 1628–1632.
- [7] M. Catti, S. Stramare, Solid State Ionics 136, 137 (2000) 489–494.
- [8] Enrique R. Losilla, Miguel A.G. Aranda, María Martínez-Lara, Sebastian Bruque, Chemistry of Materials 9 (1997) 1678–1685.
- [9] K. Arbi, M. Ayadi-Trabelsi, J. Sanz, Journal of Materials Chemistry 12 (2002) 2985–2990.
- [10] J. Kuwano, et al., Solid State Ionics 70–71 (1994) 332–336.
- [11] K. Nomura, et al., Solid State Ionics 61 (1993) 293–301.
- [12] H. Xie, Y. Li, J.B. Goodenough, RSC Advances 1 (2011) 1728–1731.
- [13] H. Xie, J.B. Goodenough, Y. Li, Journal of Power Sources 196 (2011) 7760–7762.
- [14] M. Forsyth, S. Wong, et al., Solid State Ionics 124 (3, 4) (1999) 213–219.
- [15] Y. Li, et al., Journal of Materials Chemistry 22 (2012) 15357–15361.
- [16] V. Thangadurai, W. Weppner, Journal of Power Sources 142 (2005) 339–344.
- [17] R. Murugan, V. Thangadurai, W. Weppner, Angewandte Chemie-International Edition 46 (2007) 7778–7781.
- [18] M.A. Subramanian, R. Subramanian, A. Clearfield, Solid State Ionics 18–19 (1986) 562–569.
- [19] H. Buschmann, J. Dolle, et al., Physical Chemistry Chemical Physics 13 (43) (2011) 19378–19392.
- [20] Asha Gupta, Ramaswamy Murugan, M. Parans paranthaman, et al., Journal of Power Sources 209 (2012) 184–188.